The Hard X-ray 20-40 keV AGN Luminosity Function

V. Beckmann[1]
NASA Goddard Space Flight Center, Exploration of the Universe Division, Code 661, Greenbelt, MD 20771, USA
beckmann@milkyway.gsfc.nasa.gov

S. Soldi[2,3], C. R. Shrader[4,5], N. Gehrels[4], and N. Produit[2]

ABSTRACT

We have compiled a complete, significance limited extragalactic sample based on $\sim 25,000\,\mathrm{deg}^2$ to a limiting flux of $3 \times 10^{-11}\,\mathrm{ergs\,cm^{-2}\,s^{-1}}$ ($\sim 7,000\,\mathrm{deg}^2$ to a flux limit of $10^{-11}\,\mathrm{ergs\,cm^{-2}\,s^{-1}}$) in the 20 – 40 keV band with *INTEGRAL*. We have constructed a detailed exposure map to compensate for effects of non-uniform exposure. The flux-number relation is best described by a power-law with a slope of $\alpha = 1.66 \pm 0.11$. The integration of the cumulative flux per unit area leads to $f_{20-40\,\mathrm{keV}} = 2.6 \times 10^{-10}\,\mathrm{ergs\,cm^{-2}\,s^{-1}\,sr^{-1}}$, which is about 1% of the known 20 – 40 keV X-ray background. We present the first luminosity function of AGN in the 20–40 keV energy range, based on 68 extragalactic objects detected by the imager IBIS/ISGRI on-board *INTEGRAL*. The luminosity function shows a smoothly connected two power-law form, with an index of $\gamma_1 = 0.9$ below, and $\gamma_2 = 2.2$ above the turn-over luminosity of $L_* = 4.6 \times 10^{43}\,\mathrm{ergs\,s^{-1}}$. The emissivity of all *INTEGRAL* AGNs per unit volume is $W_{20-40\,\mathrm{keV}}(> 10^{41}\,\mathrm{ergs\,s^{-1}}) = 2.8 \times 10^{38}\,\mathrm{ergs\,s^{-1}\,h_{70}^3\,Mpc^{-3}}$. These results are consistent with those derived in the 2 – 20 keV energy band and do not show a significant contribution by Compton-thick objects. Because the sample used in this study is truly local ($\bar{z} = 0.022$), only limited conclusions can be drawn for the evolution of AGNs in this energy band. But the objects explaining the peak in the cosmic X-ray background are likely to be either low luminosity AGN ($L_X < 10^{41}\,\mathrm{ergs\,s^{-1}}$) or of other type, such as intermediate mass black holes, clusters, and star forming regions.

Subject headings: galaxies: active — gamma rays: observations — X-rays: galaxies — surveys — galaxies: Seyfert

1. Introduction

The Galactic X-ray sky is dominated by accreting binary systems, while the extragalactic sky shows mainly active galactic nuclei (AGN) and clusters of galaxies. Studying the population of sources in this energy range has been a challenge ever since the first observations by rocket borne X-ray detectors (Giacconi et al. 1962). At soft X-rays (0.1 – 2.4 keV) the *ROSAT* All-Sky Survey (RASS; Voges et al. 1999) has revealed an extragalactic population of mainly broad line AGNs, such as type Seyfert 1 and quasars. Between a

[1]also with the Joint Center for Astrophysics, Department of Physics, University of Maryland, Baltimore County, MD 21250, USA

[2]INTEGRAL Science Data Centre, Chemin d' Écogia 16, 1290 Versoix, Switzerland

[3]also with Observatoire de Genève, 51 Ch. des Maillettes, 1290 Sauverny, Switzerland

[4]NASA Goddard Space Flight Center, Exploration of the Universe Division, Code 661, Greenbelt, MD 20771, USA

[5]also with Universities Space Research Association, 10211 Wincopin Circle, Columbia, MD 21044, USA

few keV and $\sim$ 1 MeV, no all-sky survey using imaging instruments has been performed to date. In the 2 - 10 keV range surveys based on significant fractions of the sky have been carried out with *ASCA* (e.g. Ueda et al. 2001), *XMM-Newton* (e.g. Hasinger 2004), and *Chandra* (e.g. Brandt et al. 2001) and have shown that the dominant extragalactic sources are more strongly absorbed than those within the RASS energy band, thus more Seyfert 2 type objects are detectable here. For a summary on the deep X-ray surveys below 10 keV see Brandt & Hasinger (2005). At higher energies the data become more scarce. The *Rossi X-ray Timing Explorer* (*RXTE*) sky survey in the $3-20$ keV energy band revealed 100 AGNs, showing an ever higher fraction of absorbed sources of about 60% (Sazonov & Revnivtsev 2004). A similar study at energies above 20 keV had not been possible, because a large field of view in combination with sufficient sensitivity are required to study the AGN population on a relevant fraction of the sky. The *International Gamma-Ray Astrophysics Laboratory* (*INTEGRAL*; Winkler et al. 2003) offers an unprecedented $>$ 20 keV collecting area and state-of-the-art detector electronics and background rejection capabilities. Notably, the imager IBIS with an operating range from $20-1000$ keV and a fully-coded field of view of $10^\circ \times 10^\circ$ enables us now to study a large portion of the sky. A first catalog of AGNs showed a similar fraction of absorbed objects as the *RXTE* survey (Beckmann et al. 2006a).

Related to the compilation of AGN surveys in the hard X-rays is the question of what sources form the cosmic X-ray background (CXB). While the CXB below 20 keV has been the focus of many studies, the most reliable measurement in the 10 - 500 keV has been provided by the *High Energy Astronomical Observatory* (*HEAO 1*), launched in 1977 (Marshall et al. 1980). The most precise measurement provided by the UCSD/MIT Hard X-ray and Gamma-Ray instrument (*HEAO 1* A-4) shows that the CXB peaks at an energy of about 30 keV (Gruber et al. 1999). The isotropic nature of the X-ray background points to an extragalactic origin, and as the brightest persistent sources are AGNs, it was suggested earlyon that those objects are the main source of the CXB (e.g. Zdziarski 1996). In the soft X-rays this concept has been proven to be correct through the observations of the *ROSAT* deep X-ray surveys, which showed that 90% of the $0.5-2.0$ keV CXB can be resolved into AGNs (Miyaji, Hasinger & Schmidt 2000). At higher energies ($2-10$ keV), *ASCA* and *Chandra* surveys measured the X-ray luminosity function (XLF). These studies show that in this energy range the CXB can be explained by AGNs, but with a higher fraction of absorbed ($N_H > 10^{22}\,\mathrm{cm}^{-2}$) objects than in the soft X-rays (e.g. Ueda et al. 2003). A study based on the *RXTE* survey by Sazonov & Revnivtsev (2004) derived the hard X-ray luminosity function of AGNs. They showed that the summed output of AGNs in this energy range is too small to explain the CXB, and suggested that a comparable X-ray flux may be produced together by lower luminosity AGNs, non-active galaxies and clusters of galaxies.

With the on-going observations of the sky by *INTEGRAL*, a sufficient amount of data is now available to derive the AGN hard X-ray luminosity function. In this paper we present analysis of recent observations performed by the *INTEGRAL* satellite, and compare the results with previous studies. In Section 2 we describe the AGN sample and in Section 3 the methods to derive the number-flux distribution of *INTEGRAL* AGNs are presented together with the analysis of their distribution. Section 4 shows the local luminosity function of AGNs as derived from our data, followed by a discussion of the results in Section 5.

2. The *INTEGRAL* AGN Sample

Observations in the X-ray to soft gamma-ray domain have been performed by the instruments on-board the *INTEGRAL* satellite (Winkler et al. 2003). This mission offers the unique potential to perform simultaneous observations over the $2-8000$ keV energy region. This is achieved by the X-ray monitor (2–30 keV) JEM-X (Lund et al. 2003), the soft gamma-ray imager (20–1000 keV) ISGRI (Lebrun et al. 2003), and the spectrograph SPI (Vedrenne et al. 2003), which operates in the 20 – 8000 keV region. Each of these instruments employs the coded-aperture technique (Caroli et al. 1987). In addition to these data an optical monitor (OMC, Mas-Hesse et al. 2003) provides photometric measurements in the V band.

Data used for the analysis presented here were all in the public domain by the end of March 2005. This includes data from orbit revolutions 19 - 137 and revolutions 142 - 149. Data before revolution 19 have been excluded as the instruments settings changed frequently and therefore the data from this period are not suitable to be included into a homogeneous survey.

The list of sources was derived from the analysis as described in Beckmann et al. (2006a). Additional observations performed later led to further source detections within the survey area. We extracted spectra at those positions from the data following the same procedure. It is understood that most of those objects did not result in a significant detection in the data set used here, but it ensures completeness of the sample at a moderate significance limit.

The analysis was performed using the Offline Science Analysis (OSA) software version 5.0 distributed by the ISDC (Courvoisier et al. 2003a). We applied the same method for IBIS/ISGRI and SPI analysis as described in Beckmann et al. (2006a). The analysis of the *INTEGRAL*/IBIS data is based on a cross-correlation procedure between the recorded image on the detector plane and a decoding array derived from the mask pattern (Goldwurm et al. 2003). The ISGRI spectra have been extracted from the count rate and variance mosaic images at the position of the source, which in all cases corresponds to the brightest pixel in the $20 - 40\,\mathrm{keV}$ band.

The significances listed in Tab. 1 have been derived by using the OSA software, and refer to the count rate and count rate error for ISGRI in the 20 - 40 keV energy band. The luminosities listed are the observed luminosities in this energy band. The absorption listed is the intrinsic absorption in units of $10^{22}\,\mathrm{cm}^{-2}$ as measured in soft X-rays by various missions as referenced. We also include the most important reference for the *INTEGRAL* data of the particular source in the last column of Table 1. The extracted images and source results are available in electronic form[1].

In order to provide a complete list of AGNs detected by *INTEGRAL*, we included also those sources which are not covered by the data used for our study. Those sources are marked in Tab. 1 and are not used in our analysis.

[1] http://heasarc.gsfc.nasa.gov/docs/integral/inthp_archive.html

3. Number-Flux Distribution of *INTEGRAL* AGNs

In order to compute the AGN number-flux relation counts of AGNs it is necessary to have a complete and unbiased sample, and to know the characteristics of the survey used to extract the data. Because of the in-homogeneous character of the survey, we had to apply a significance limit rather than a flux limit to define a complete sample. The task is to find a significance limit which ensures that all objects above the given limit have been found. To test for completeness, the V_e/V_a-test has been applied.

The V_e/V_a-test is a simple method developed by Avni & Bahcall (1980) based on the V/V_{max} test of Schmidt (1968). V_e stands for the volume, which is enclosed by the object, and V_a is the accessible volume, in which the object could have been found (e.g. due to a flux limit of a survey). Avni & Bahcall showed that different survey areas with different flux limits in various energy bands can be combined by the V_e/V_a-test. In the case of no evolution $\langle V_e/V_a \rangle = 0.5$ is expected. This evolutionary test is applicable only to samples with a well-defined significance limit down to which all objects have been found. It can therefore also be used to test the completeness of a sample. We performed a series of V_e/V_a-tests to the *INTEGRAL* AGN sample, assuming completeness limits in the range of 1σ up to 6σ ISGRI 20 - 40 keV significance. For a significance limit below the true completeness limit of the sample one expects the V_e/V_a-tests to derive a value $\langle V_e/V_a \rangle < \langle V_e/V_a \rangle_{true}$, where $\langle V_e/V_a \rangle_{true}$ is the true test result for a complete sample. Above the completeness limit the $\langle V_e/V_a \rangle$ values should be distributed around $\langle V_e/V_a \rangle_{true}$ within the statistical uncertainties. An example of this method to determine the significance limit can be found in Beckmann et al. (2006a).

It appears that the sample becomes complete at a significance cutoff of approximately 5σ, which includes 38 AGNs. The average value is $\langle V_e/V_a \rangle = 0.45 \pm 0.05$. This is consistent with the expected value of 0.5 which reflects no evolution and an even distribution in the local universe.

A pure number flux distribution (i.e. $\log N_{>S}$

versus $\log S$) for the sample presented here would not give meaningful results, because of the different exposure times across the survey, and therefore the varying sensitivity within the survey. An uncorrected number flux distribution for *INTEGRAL* AGNs has been shown in Beckmann et al. (2006b). To correct for the different exposure times it is necessary to count the number of AGNs per unit sky area. Thus the number of AGNs above a given flux have to be counted and divided by the sky area in which they are detectable throughout the survey. We therefore first determined the exposure time in 64,620 sky elements of $\sim 0.63\,\mathrm{deg}^2$ size within our survey. In each sky bin, the exposure is the sum of each individual exposure multiplied by the fraction of the coded field of view in this particular direction. The dead time and the good time intervals (GTI) are not taken into account but the dead time is fairly constant (around 20%) and GTI gaps are very rare in IBIS/ISGRI data. Figure 1 shows the exposure map in Galactic coordinates for this survey. We excluded those fields with an exposure time less than 2 ks, resulting in 47,868 sky elements with a total coverage of 9.89 sr. The flux limit for a given significance limit should be a function of the square root of the exposure time, if no systematic effects apply, but this assumption cannot be made here. The nature of coded-mask imaging leads to accumulated systematic effects at longer exposure times. In order to achieve a correlation between the exposure time and the flux limit, we therefore used an empirical approach. We correlated the exposure time of each object with an equivalent flux correspoding to 5σ significance based on the flux and significance of each sample object. By using only the AGNs of our survey we are additionally assured to consider effects based on the spectral slope (for AGNs $\Gamma \simeq 2$). The correlation was then fit by a smooth polynomial (Fig. 2). This function was then used to estimate the flux limit of each survey field. It has to be noted that the individual flux limit of each survey field is not important, but only the correct distribution of those flux limits. The total area in the survey for a given flux limit is shown in Figure 3.

Based on the flux limits for all survey fields, we are now able to construct the number flux distribution for the *INTEGRAL* AGN, determining for each source flux the total area in which the source is detectable with a 5σ detection significance in the $20-40$ keV energy band. The resulting correlation is shown in Fig. 4.

3.1. The Slope of the Number-Flux Distribution

We applied a maximum-likelihood (ML) algorithm to our empirical number-flux distribution to obtain a power-law approximation of the form $N(>S) = K \cdot S^{-\alpha}$. Our approach was based on the formalism derived by Murdoch, Crawford and Jauncey (1973), also following the implementation of Piccinotti et al (1982). The latter involved modification of the basic ML incorporated to facilitate handling of individual source flux-measurement errors. The ML method also involves the application of a Kolmogorov-Smirnov (K-S) test to evaluate the goodness of fit, as detailed in Murdoch, Crawford and Jauncey (1973). Once the slope is determined, a chi-square minimization is used to deterimine the amplitude K.

For this analysis, we used a sub-sample of 38 sources for which the statistical significance of our flux determinations was at a level of 5σ or greater. The dimmest source among this sub-sample was $f_X = 5.6 \times 10^{-12}\,\mathrm{ergs\,cm^{-2}\,s^{-1}}$, and the brightest was $f_X = 3.2 \times 10^{-10}\,\mathrm{ergs\,cm^{-2}\,s^{-1}}$. We derived a ML probability distribution, which can be approximated by a Gaussian, with our best fit parameters of $\alpha = 1.66 \pm 0.11$. A normalization of $K = 0.44\,\mathrm{sr^{-1}}\,(10^{-10}\,\mathrm{ergs\,cm^{-2}\,s^{-1}})^{\alpha}$ was then obtained by performing a least-squares fit, with the slope fixed to the ML value.

4. The Local Luminosity Function of AGNs at 20 – 40 keV

The complete sample of *INTEGRAL* AGNs with a detection significance $\geq 5\sigma$ also allows us to derive the density of these objects in the local Universe as a function of their luminosity. In order to derive the density of objects above a given luminosity, one has to determine for each source in a complete sample the space volume in which this source could have been found considering both the flux limit of each survey field and the apparent brightness of the object. We have again used the correlation between exposure time and flux limit as discussed in the previous section in order to assign a 5σ flux limit to each survey field. Then the

maximum redshift z_{max} at which an object with flux f_X would have been detectable in each sky element was used to compute the total accessible volume

$$V_a = \sum_{i=1}^{N} \frac{\Omega_i}{4\pi} V_i[z_{max,i}(f_X)] \quad (1)$$

with N being the number of sky elements in which the object would have been detectable and Ω_i the solid angle covered by sky element i. We applied a cosmology with $H_0 = 70\,\mathrm{km\,s^{-1}\,Mpc^{-1}}$ ($h_{70} = 1$), $k = 0$ (flat Universe), $\Omega_{matter} = 0.3$, and $\Lambda_0 = 0.7$, although a $\Lambda_0 = 0$ and $q_0 = 0.5$ cosmology does not change the results significantly because of the low redshifts in our sample. Figure 5 shows the cumulative luminosity function for 38 *INTEGRAL* detected ($\geq 5\sigma$) AGNs in the 20 – 40 keV energy band. Here the density ϕ describes the number of objects per Mpc^3 above a given luminosity L_X: $\phi = \sum_{i=1}^{K} V_{a,i}^{-1}$ with K being the number of objects with luminosities $> L_X$. Blazars have been excluded because their emission is not isotropic. The redshifts in the sample range from $z = 0.001$ to $z = 0.129$ with an average redshift of $\bar{z} = 0.022$. Thus the luminosity function is truly a local one. Figure 6 shows the luminosity function in differential form, indicating that the sample indeed does not show luminosity bins with large incompleteness compared to the rest of the sample. The errors are based on the number of objects contributing to each value. The differential XLF also shows, like the cumulative one, a turnover around $L_X = (5 - 10) \times 10^{43}\,\mathrm{ergs\,s^{-1}}$.

Because our study is based solely on low redshift objects, we are not able to constrain models involving evolution with redshift. Nevertheless we can compare the XLF presented here with model predictions from previous investigations. XLFs are often fit by a smoothly connected two power-law function of the form (Maccacaro et al. 1991)

$$\frac{d\phi(L_X, z=0)}{d\log L_X} = A\left[\left(\frac{L_X}{L_*}\right)^{\gamma_1} + \left(\frac{L_X}{L_*}\right)^{\gamma_2}\right]^{-1} \quad (2)$$

We fit this function using a least-squares method applying the Levenberg-Marquardt algorithm. The best fit values we obtained are $A = (2.7\pm0.5)\times10^{-6}\,h_{70}^3\,\mathrm{Mpc^{-3}}$, $\gamma_1 = 0.93\pm0.15$, $\gamma_2 = 2.23\pm0.15$, and $L_* = (4.6\pm2.0)\times10^{43}\,h_{70}^{-2}\,\mathrm{ergs\,s^{-1}}$. The errors have been estimated on the basis of the uncertainties of the density determination and of the flux measurement. These values are consistent with values derived from the $2-10\,\mathrm{keV}$ XLF of AGNs as shown by e.g. Ueda et al. (2003) and La Franca et al. (2005). For example the work by Ueda et al. (2003) reveals for a pure density evolution model the same values for A, γ_1, and γ_2, but a higher $L_* = 1.29 \times 10^{44}\,\mathrm{erg\,s^{-1}}$. This ratio of 2.8 in the turnover luminosity can be easily explained by the different energy bands applied. A single power law with photon index of $\Gamma = 1.9$ in the range $2 - 40\,\mathrm{keV}$ would lead to $L_{(2-10\,\mathrm{keV})}/L_{(20-40\,\mathrm{keV})} = 2.8$, assuming no intrinsic absorption. Thus it appears that the local luminosity function of AGNs in the $20-40\,\mathrm{keV}$ band can simply be extrapolated from the $2 - 10\,\mathrm{keV}$ range. This has, of course, no implications for the XLF at higher redshifts. The values are also consistent with the luminosity function for AGNs in the $3 - 20\,\mathrm{keV}$ band as derived by Sazonov & Revnivtsev (2004) from the *RXTE* all-sky survey.

Information about intrinsic absorption is available for 34 of the 38 objects (89%) from soft X-ray observations. This enables us to derive the luminosity function for absorbed ($N_H \geq 10^{22}\,\mathrm{cm^{-2}}$) and unabsorbed sources, as shown in Figure 7. The absorbed sources have a higher density than the unabsorbed sources at low luminosities, while this trend is inverted at high luminosities. The luminosity where both AGN types have similar densities is about $L_{(20-40\,\mathrm{keV})} = 3\times10^{43}\,\mathrm{erg\,s^{-1}}$. This tendency is also evident when comparing the fraction of absorbed AGNs with the luminosity in the three luminosity bins depicted in Figure 8. The luminosity bins have been chosen so that an equal number of objects are contained in each bin. The position of the data point along the luminosity axis indicates the average luminosity in this bin, while the error bars in luminosity indicate the range of luminosities covered.

Based on the luminosity function, the contribution of the AGNs to the total X-ray emissivity W can be estimated (Sazonov & Revnivtsev 2004). This can be done by simply multiplying the XLF by the luminosity in each bin and integrating over the range of luminosities ($10^{41}\,\mathrm{ergs\,s^{-1}} < L_{20-40\,\mathrm{keV}} < 10^{45.5}\,\mathrm{ergs\,s^{-1}}$). This results in $W_{20-40\,\mathrm{keV}}(> 10^{41}\,\mathrm{ergs\,s^{-1}}) = 2.8\times10^{38}\,\mathrm{ergs\,s^{-1}\,h_{70}^3\,Mpc^{-3}}$.

5. Discussion

The number flux distribution (Fig. 4) shows a slope of $\alpha = 1.66 \pm 0.11$. In the local Universe with no evolution,and isotropic distribution of AGN and assuming Eucledian geometry, the expected value is $\alpha = 1.5$ Even though the difference is only significant on a 1.5σ level, this might indicate that the area density at the low flux end of the distribution has been slightly overcorrected. One has to keep in mind that only a few sources derived from a small area of the sky are constraining the low flux end. Krivonos et al. (2005) studied the extragalactic source counts as observed by *INTEGRAL* in the 20-50 keV energy band in the Coma region. Based on 12 source detections they determine a surface density of $(1.4 \pm 0.5) \times 10^{-2}\,\mathrm{deg}^{-2}$ above a threshold of $10^{-11}\,\mathrm{ergs\,cm^{-2}\,s^{-1}}$ in the $20 - 50\,\mathrm{keV}$ energy band, where we get a consistent value of $(1.2 \pm 0.2) \times 10^{-2}\,\mathrm{deg}^{-2}$. Comparing the total flux of all the objects in the AGN sample ($f_{20-40\,\mathrm{keV}} = 2.6 \times 10^{-10}\,\mathrm{ergs\,cm^{-2}\,s^{-1}\,sr^{-1}}$) with the flux of the X-ray background as presented by Gruber et al. (1999) shows that the *INTEGRAL* AGN account only for about 1% of the expected value. This is expected when taking into account the high flux limit of our sample: La Franca et al. (2005) have shown that objects with $f_{2-10keV} > 10^{-11}\,\mathrm{ergs\,cm^{-2}\,s^{-1}}$ contribute less than 1% to the CXB. This flux limit translates to the faintest flux in our sample of $f_{20-40keV} = 5.6 \times 10^{-12}\,\mathrm{ergs\,cm^{-2}\,s^{-1}}$ for a $\Gamma = 1.9$ power law spectrum.

We compared the emissivity per unit volume of our objects $W_{20-40\,\mathrm{keV}}(> 10^{41}\,\mathrm{ergs\,s^{-1}}) = 2.8 \times 10^{38}\,\mathrm{ergs\,s^{-1}\,h_{70}^{3}\,Mpc^{-3}}$ with that found in the 3–20 keV band. Assuming an average power law of $\Gamma = 1.9$, the extrapolated value is $W_{3-20\,\mathrm{keV}}(> 10^{41}\,\mathrm{ergs\,s^{-1}}) = 6.7 \times 10^{38}\,\mathrm{ergs\,s^{-1}\,h_{70}^{3}\,Mpc^{-3}}$, which is a factor of 1.3 larger than the value measured by *RXTE* (Sazonov & Revnivtsev 2004) and consistent within the 1σ error. Extrapolating our result down to 2–10 keV shows an emissivity which is lower by a factor of 1.2 compared to the one derived from the *HEAO-1* all-sky map (Miyaji et al. 1994) and also within the statistical uncertainties.

The luminosity function derived from the *INTEGRAL* $20 - 40\,\mathrm{keV}$ AGN sample appears to be consistent with the XLF in the $2 - 20\,\mathrm{keV}$ range. A turnover in the XLF at $\simeq 4.6 \times 10^{43}\,\mathrm{ergs\,s^{-1}}$ is observed (Fig. 6). Below this luminosity also the fraction of absorbed AGNs starts to be larger than that of the unabsorbed ones, although the effect is significant only on a 1σ level (Fig. 7). Both effects have been seen also in the $2 - 10\,\mathrm{keV}$ (Ueda et al. 2003; La Franca et al. 2005) and in the $3-20\,\mathrm{keV}$ band (Sazonov & Revnivtsev 2004). This implies that we do detect a similar source population as at lower energies. If a large population of absorbed AGNs is dominating the cosmic X-ray background at $\sim 30\,\mathrm{keV}$ as indicated by *HEAO 1* A-4 measurements (Gruber et al. 1999), and the source population is the same throughout the Universe those objects would have to have luminosities $L_{(20-40\,\mathrm{keV})} < 10^{41}\,\mathrm{ergs\,s^{-1}}$, as might be indicated by the larger fraction of absorbed sources toward lower luminosities (Fig. 7). Even though it has to be taken into account that the low luminosity end of the XLF is based only on a small number of objects, below this luminosity the distribution between active and normal galaxies becomes blurred. Additionally objects like Ultra-luminous X-ray sources (ULX) and star-forming galaxies could provide the necessary emission. One interesting case in this category is the detection of NGC 4395 with a luminosity of $L_{(20-40\,\mathrm{keV})} = 1.4 \times 10^{40}\,\mathrm{ergs\,s^{-1}}$, consistent with measurements by *XMM-Newton* which showed $L_{(2-10\,\mathrm{keV})} = 1.5 \times 10^{40}\,\mathrm{ergs\,s^{-1}}$ (Vaughan et al. 2005). The central engine of this galaxy has been classified as an "ultra-luminous" source, possibly associatied with an intermediate mass black hole with $M_{BH} = (4^{+6}_{-3} \times 10^{4}\,\mathrm{M_{\odot}}$ (McHardy et al. 2005). In addition, NGC 4395 harbors a ULX with $L_{(2-10\,\mathrm{keV})} = 10^{39}\,\mathrm{ergs\,s^{-1}}$ at a distance of 2.9 kpc from the center of the galaxy (Colbert & Ptak 2002).

Another scenario is that the population of X-ray emitting sources depends on redshift, i.e. that there is an evolution of population in time, indicating that the fraction of absorbed sources might be higher at larger redshifts, although it should be noted that the latter effect is not clearly detectable in the $2 - 10\,\mathrm{keV}$ range. The fraction of absorbed sources seems to depend on luminosity (Ueda et al. 2003; Treister & Urry 2005), as seen also in the $20 - 40\,\mathrm{keV}$ band (Fig. 8). But some studies come to the conclusion that there is no evolution of N_H (Ueda et al. 2004;

Treister & Urry 2005), while others find the fraction of absorbed sources increasing with redshift (La Franca et al. 2005). The latter also find that a combination of effects (the fraction of absorbed AGN decreases with the intrinsic X-ray luminosity, and increases with the redshift) can be explained by a luminosity-dependent density evolution model. They further show that the luminosity function of AGNs like those presented here peaks at $z \sim 0.7$ while high luminosity AGN peak at $z \sim 2$. Unified models also predict, depending on the applied model, a fraction of $0.6 - 0.7$ for high flux low redshift AGN (Treister & Urry 2005). Worsley et al. (2005) examined *Chandra* and *XMM-Newton* deep fields and come to the conclusion that the missing CXB component is formed by highly obscured AGNs at redshifts $\sim 0.5 - 1.5$ with column densities of the order of $f_X = 10^{23} - 10^{24}\,\mathrm{cm}^{-2}$. Evidence for this scenario is also found in a study of *Chandra* and *Spitzer* data (Polletta et al. 2006). Combining multiwavelength data, this work estimates a surface density of $25\,\mathrm{AGN\,deg}^{-2}$ in the infrared in the $0.6\,\mathrm{deg}^2$ *Chandra*/SWIRE field, and only 33% of them are detected in the X-rays down to $f_{0.3-8\,\mathrm{keV}} = 10^{-15}\,\mathrm{ergs\,cm}^{-2}\,\mathrm{s}^{-1}$. The work also indicates a higher abundance of luminous and Compton-thick AGN at higher redshifts ($z \gg 0.5$). This source population would be missed by the study presented here, because of the low redshifts ($\bar{z} = 0.022$) of the *INTEGRAL* AGNs.

Several studies (Ueda et al. 2004; Treister & Urry 2005) propose that the absorbed AGNs needed to explain the CXB should be Compton thick, and therefore would have been missed at $2 - 10\,\mathrm{keV}$. This argument does not hold for the *INTEGRAL* observations, where the impact of absorption is much less severe than at lower energies. The effect on the measured flux of a source with photon index $\Gamma = 2$ for Compton thick absorption ($N_H = 10^{24}\,\mathrm{cm}^{-2}$) is only a 5% decrease in flux (40% for $N_H = 10^{25}\,\mathrm{cm}^{-2}$). It is therefore unlikely that many Compton-thick objects have been missed by the *INTEGRAL* studies performed to date. One possibility would be, that they are among the newly detected sources found by *INTEGRAL*. The fraction of unidentified objects among those sources is of the order of 50%. It should be pointed out though, that most of these sources are located close to the Galactic plane and are more likely to belong to the Galaxy: the Second IBIS/ISGRI Soft Gamma-Ray Survey Catalog (Bird et al. 2006) lists 55 new sources detected by *INTEGRAL*, of which 93% are located within $-10° < b < +10°$. Among those sources 3 are listed as extragalactic sources, 18 are of Galactic origin, and 29 have not been identified yet.

In addition, those objects which have been demonstrated to be AGNs, are no more likely to be Compton-thick objects than the overall AGN population studied here. Only four AGNs (NGC 1068, NGC 4945, MRK 3, Circinus galaxy) detected by *INTEGRAL* have been proven to be Compton thick objects so far, and none of them showed absorbtion of $N_H > 5 \times 10^{24}\,\mathrm{cm}^{-2}$. In order to clarify this point, observations at soft X-rays of those objects without information about intrinsic absorption are required for all *INTEGRAL* detected AGNs (Tab. 1). Up to now 23 % of the *INTEGRAL* AGN are missing absorption information. A first indication of what the absorption in these sources might be, can be derived from comparison of the *INTEGRAL* fluxes with *ROSAT* All-Sky Survey (RASS) Faint Source Catalogue data (Voges et al. 2000). In order to do so we assumed a simple power law with photon index $\Gamma = 2.0$ between the *ROSAT* $0.1 - 2.4\,\mathrm{keV}$ band and the *INTEGRAL* $20 - 40\,\mathrm{keV}$ range and fit the absorption. In the six cases where no detection was achieved in the RASS, an upper limit of $f_{(0.1-2.4\,\mathrm{keV})} \leq 10^{-13}\,\mathrm{ergs\,cm}^{-2}\,\mathrm{s}^{-1}$ has been assumed, resulting in a lower limit for the absorption $N_H > (5-11) \times 10^{22}\,\mathrm{cm}^{-2}$. In Fig. 9 we show the distribution of intrinsic absorption. It has to be pointed out that the estimated values can only give an idea about the distribution of intrinsic absorption and should not be taken literally, as the spectral slope between the measurements is unknown and the observations are not simultaneous. Nevertheless apparently none of the RASS detections and non-detections requires an intrinsic absorption of $N_H > 2 \times 10^{23}\,\mathrm{cm}^{-2}$. Therefore it appears unlikely that a significant fraction of *INTEGRAL* AGNs will show an intrinsic absorption $N_H > 10^{24}\,\mathrm{cm}^{-2}$. A similar result in the $3-20\,\mathrm{keV}$ band let Sazonov & Revnivtsev (2004) to the conclusion that the missing emission to explain the CXB is not produced in 'normal' AGNs, but that a comparable X-ray flux might be produced together by low luminosity AGNs, non-active galax-

ies and clusters of galaxies.

Most investigations have been focused so far on the X-rays below 20 keV, and *INTEGRAL* can add substantial information to the nature of bright AGNs in the local Universe. Considering the expected composition of the hard X-ray background, it does not currently appear that the population detected by *INTEGRAL* can explain the peak at 30 keV, as Compton thick AGNs are apparently less abundant than expected. But the sample presented here might be still too small to constrain the fraction of obscured sources, and the missing Compton thick AGN could be detected when studying sources with $f_{(20-40\,\mathrm{keV})} < 10^{-11}\,\mathrm{ergs\,cm^{-2}\,s^{-1}}$.

6. Conclusions

A statistically complete extragalactic sample derived from the *INTEGRAL* public data archive comprises 58 low redshift Seyfert galaxies ($\langle z \rangle = 0.022 \pm 0.003$) and 8 blazars in the hard X-ray domain. Two galaxy clusters are also detected, but no star-burst galaxy has been as yet. This *INTEGRAL* AGN sample is thus the largest one presented so far.

The number flux distribution shows a slope of $\alpha = 1.66 \pm 0.11$. Because of the high flux limit of our sample the objects account in total for less than 1% of the $20 - 40\,\mathrm{keV}$ cosmic X-ray background. The emissivity of all AGNs per unit volume $W_{20-40\,\mathrm{keV}}(> 10^{41}\,\mathrm{ergs\,s^{-1}}) = 2.8 \times 10^{38}\,\mathrm{ergs\,s^{-1}\,h_{70}^{3}\,Mpc^{-3}}$ appears to be consistent with the background measurements in the 2–10 keV energy band.

The luminosity function in the $20 - 40\,\mathrm{keV}$ energy range is consistent with that measured in the $2 - 20\,\mathrm{keV}$ band. Below the turnover luminosity of $L_* = 4.6 \times 10^{43}\,\mathrm{ergs\,s^{-1}}$ the absorbed AGNs become dominant over the unabsorbed ones. Only a small fraction of Compton thick AGNs are detectable within the sample with known intrinsic absorption. For the sources without reliable absorption information we derived an estimate from the comparison with *ROSAT* All-Sky Survey data and find that the data do not require additional Compton thick objects within the sample presented here. The sources to explain the 30 keV peak in the cosmic X-ray background have to be either at higher redshift, as proposed for example by Worsley et al. (2005), which would imply an evolution towards stronger absorption with redshift, or the missing emission has to be due to low luminosity AGNs, clusters of galaxies, non-active galaxies or ultra-luminous X-ray sources.

Over the life time of the *INTEGRAL* mission we expect to detect of the order of 200 AGNs. Combining these data with the studies based on *Swift*/BAT, operating in a similar energy band as IBIS/ISGRI, will further constrain the hard X-ray luminosity function of AGNs. But we will still be limited to relatively the high flux, low luminosity and low redshift end of the distribution, which will be inadequate to explain the cosmic X-ray background at $E > 20\,\mathrm{keV}$. Future missions such as *EXIST* or *NuStar* will be required to answer the question of what dominates the Universe in the hard X-rays.

VB would like to thank Olaf Wucknitz for providing software to handle the $\Lambda_0 > 0$ cosmology. This research has made use of the NASA/IPAC Extragalactic Database (NED) which is operated by the Jet Propulsion Laboratory, of data obtained from the High Energy Astrophysics Science Archive Research Center (HEASARC), provided by NASA's Goddard Space Flight Center, and of the SIMBAD Astronomical Database which is operated by the Centre de Données astronomiques de Strasbourg. This research has made use of the Tartarus (Version 3.1) database, created by Paul O'Neill and Kirpal Nandra at Imperial College London, and Jane Turner at NASA/GSFC. Tartarus is supported by funding from PPARC, and NASA grants NAG5-7385 and NAG5-7067.

REFERENCES

Avni, Y. & Bahcall, J. N. 1980, ApJ, 235, 694

Barger, A. J., Cowie, L. L., Mushotzky, R. F., Yang, Y., Wang, W.-H., Steffen, A. T., & Capa, P. 2005, AJ, 129, 578

Bassani, L., et al. 2006, ApJ, 636, L65

Beckmann, V., Gehrels, N., Favre, P., Walter, R., Courvoisier, T. J.-L., Petrucci, P.-O., Malzac, J. 2004, ApJ, 614, 641

Beckmann, V., et al. 2005, ApJ, 634, 939

Beckmann, V., Gehrels, N., Shrader, C. R., & Soldi, S. 2006, ApJ, 638, 642

Beckmann, V., Soldi, S., Shrader, C. R., & Gehrels, N. 2006, proc. of "The X-ray Universe 2005", San Lorenzo de El Escorial (Madrid, Spain), 26-30 September 2005, ESA-SP 604, astro-ph/0510833

Bird, A., et al. 2006, ApJ, 636, 765

Brandt, W. N., et al. 2001, AJ, 122, 2810

Brandt, W. N., & Hasinger, G. 2005, ARA&A, 43

Caroli, E., Stephen, J. B., Di Cocco, G., Natalucci, L., Spizzichino, A. 1987, Space Sci. Rev., 45, 349

Colbert, E. J. M., & Ptak, A. F. 2002, ApJSS, 143, 25

Comastri, A., Fiore, F., Vignali, C., Matt, G., Perola, G. C., & La Franca, F. 2001, MNRAS, 327, 781

Courvoisier, T.J.-L., et al. 2003a, A&A, 411, L53

Courvoisier, T.J.-L., et al. 2003b, A&A, 411, L343

De Rosa, A., et al. 2005, A&A, 438, 121

Donato, D., Sambruna, R. M., Gliozzi, M. 2005, A&A, 433, 1163

Giacconi, R., Gursky, H., Paolini, R., & Rossi, B. 1962, Phys. Rev. Lett.,9,439

Gilli, R., Risaliti, G., & Salvati, M. 1999, A&A, 347, 424

Goldwurm, A., et al. 2003, A&A, 411, L223

Gruber, D. E., Matteson, J. L., Peterson, L. E., & Jung, G. V. 1999, ApJ, 520, 124

Hasinger, G. 2004, Nucl. Phys. B (Proc. Suppl.), 132, 86

Krivonos, R., Vikhlinin, A., Churazov, E., Lutovinov, A., Molkov, S., & Sunyaev, R. 2005, ApJ, 625, 89

La Franca, F., et al. 2005, ApJ, 635, 864

Lebrun, F., et al. 2003, A&A, 411, L141

Levenson, N. A., Weaver, K. A., & Heckman, T. M. 2001, ApJS, 133, 269

Lund, N., et al. 2003, A&A, 411, L231

Lutz, D., Maiolino, R., Spoon, H. W. W., Moorwood, A. F. M. 2004, A&A, 418, 465

Maccacaro, T., Della Ceca, R., Gioia, I. M., Morris, S. L., Stocke, J. T., & Wolter, A. 1991, 374, 117

Marshall, F. E., et al. 1980, ApJ, 235, 4

Mas-Hesse, J. M., et al. 2003, A&A, 411, L261

Masetti, N., Palazzi, E., Bassani, L., Malizia, A., Stephen, J. B. 2004, A&A, 426, L41

Masetti, N., 2006, A&A accepted, astro-ph/0512399

Matsumoto, C., Nava, A., Maddox, L. A., Leighly, K. M., Grupe, D., Awaki, H., Ueno, S. 2004, ApJ, 617, 930

Matt, G., et al. 1997, A&A, 325, L13

McHardy, I. M. M., Gunn, K. F., Uttley, P., & Goad, M. R. 2005, MNRAS, 359, 1469

Miyaji, T., Hasinger, G., & Schmidt, M. 2000, A&A, 353, 25

Miyaji, T., Lahav, O., Jahoda, K., & Boldt, E. 1994, ApJ, 434, 424

Murdoch, H.S., Crawford, D.F., & Jauncey, D.L. 1973, ApJ, 183, 1

Pian, E., et al. 2005, A&A, 429, 427

Pian, E., et al. 2006, A&A letters accepted, astro-ph/0602268

Piccinotti, G., Mushotzky, R. F., Boldt, E. A., Holt, S. S., Marshall, F. E., Serlemitsos, P. J., & Shafer, R. A. 1982, ApJ, 253, 485

Polletta, M., et al. 2006, ApJ accepted, astro-ph/0602228

Revnivtsev, M. G., et al. 2004, AstL, 30, 328

Revnivtsev, M. G., Sazonov, S. Yu., Molkov, S. V., Lutovinov, A. A., Churazov, E. M., & Sunyaev, R. A. 2005, Astronomy Letters accepted, astro-ph/0508155

Sazonov, S. Y., Revnivtsev, M. G., Lutovinov, A. A., Sunyaev, R. A., & Grebenev, S. A. 2004, A&A, 421, L21

Sazonov, S. Y. & Revnivtsev, M. G. 2004, A&A, 423, 469

Sazonov, S. Y., Churazov, E., Revnivtsev, M. G., Vikhlinin, A., Sunyaev, R., 2005, A&A, 444, L37

Schmidt, M., 1968, ApJ, 151, 393

Soldi, S., et al. 2005, A&A, 444, 431

Treister, E., & Urry, C. M. 2005, ApJ, 630, 115

Ueda, Y., Akiyama, M., Ohta, K., & Miyaji, T. 2003, ApJ, 598, 886

Ueda, Y., Akiyama, M., Ohta, K., & Miyaji, T. 2004, PThPS, 155, 209

Ueda, Y., Ishisaki, Y., Takahashi, T., Makishima, K., & Ohashi, T. 2001, ApJS, 133, 1

Vaughan, S., Iwasawa, K., Fabian, A. C., & Hayashida, K. 2004, MNRAS, 356, 524

Vedrenne, G., et al. 2003, A&A, 411, L63

Virani, S. N., et al. 2005, AAS, 207, 2007

Voges, W., et al. 1999, A&AS, 349, 389

Voges, W., et al. 2000, IAUC, 7432, 3

Winkler, C., et al. 2003, A&A, 411, L1

Worsley, M. A., et al. 2005, MNRAS, 357, 1281

Young, A. J., Wilson, A. S., Terashima, Y., Arnaud, K. A., Smith, D. A. 2002, ApJ, 564, 176

Zdziarski, A. A. 1996, MNRAS, 281, L9

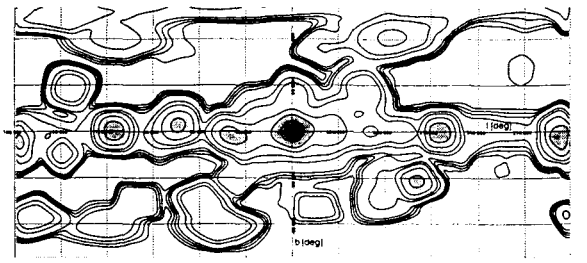

Fig. 1.— Exposure map representing the data used in our analysis in Galactic coordinates. Contours indicate 2 ks, 5 ks, 10 ks, 20 ks, 100 ks, 200 ks, 500 ks, 1 Ms, 2 Ms exposure time. *INTEGRAL* spent most of the observing time on and near the Galactic plane, with a strong focus on the Galactic center and on areas including bright hard X-ray sources like the Cygnus region, Vela, GRS 1915+105, and the Crab. Fields at high Galactic latitude include Coma, Virgo and the region around NGC 4151.

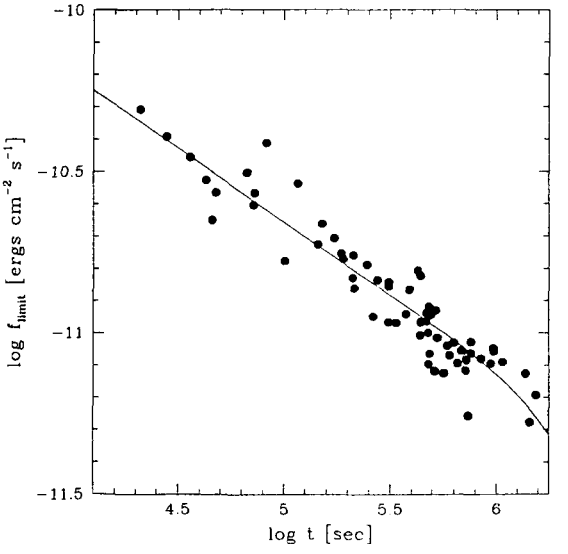

Fig. 2.— Correlation of exposure time and flux limit (5σ, $20-40\,\mathrm{keV}$) for the AGNs in this study. The curve shows a smooth polynomial fit for flux limit versus logarithm of the exposure time.

This 2-column preprint was prepared with the AAS LaTeX macros v5.2.

TABLE 1
INTEGRAL AGN CATALOG

Name	Type	z	R.A. (J2000.0)	Decl. (J2000.0)	exp.[a] (ks)	ISGRI (σ)	f_X[b]	log $L_{20-40\,keV}$ (ergs s^{-1})	N_H[c,f]	Ref.[f]
1ES 0033+595	BL Lac	0.086	00 35 53	+59 50 05	1449	3.5	0.37	43.83	0.36[1]	2
NGC 788	Sy 1/2	0.0136	02 01 06	-06 48 57	311	10.7	2.98	43.09	< 0.02[3]	4
NGC 1068	Sy 2	0.003793	02 42 41	-00 00 48	311	4.3	0.93	41.47	> 150[5]	4
QSO B0241+62	Sy 1	0.044557	02 44 58	+62 28 07	43	3.4	2.02	43.97	1.5[6]	7
NGC 1142	Sy 2	0.028847	02 55 12	-00 11 02	311	5.5	1.58	43.48	?	8
NGC 1275	Sy 2	0.017559	03 19 48	+41 30 42	264	8.4	1.89	43.12	3.75[4]	4
3C 111	Sy 1	0.048500	04 18 21	+38 01 36	67	10.0	6.27	44.54	0.63[3]	4
UGC 3142	Sy 1	0.021655	04 43 47	+28 58 19	247	16.8	5.46	43.76	?	2
LEDA 168563	Sy 1	0.0290	04 52 05	+49 32 45	28	2.8	2.27	43.64	?	2
MCG +8-11-11	Sy 1.5	0.020484	05 54 54	+46 26 22	21	6.2	6.07	43.76	< 0.02[6]	4
MRK 3	Sy 2	0.013509	06 15 36	+74 02 15	472	15.9	3.65	43.17	110[6]	4
MRK 6	Sy 1.5	0.018813	06 52 12	+74 25 37	482	8.7	2.01	43.21	10[6]	4
S5 0716+714	BL Lac	0.3[d]	07 21 53	+71 20 36	482	0.7	0.14	44.41[d]	< 0.01[3]	9
ESO 209-12	Sy 1.5	0.040495	08 01 58	-49 46 36	1543	6.7	0.86	43.52	?	7
FRL 1146	Sy 1	0.031789	08 38 31	-35 59 35	849	3.6	0.60	43.15	?	7
S5 0836+710	FSRQ	2.172	08 41 24	+70 53 42	391	6.4	1.73	47.79	0.11[3]	9
MCG-05-23-16	Sy1.9	0.008486	09 47 40	-30 56 56	2	2.3	11.20	43.25	1.6[16]	16
IGR J10404-4625	Sy 2	0.0237	10 40 22	-46 25 26	46	1.5	0.67	42.93	?	10
IGR J12026-5349	AGN	0.028	12 02 48	-53 50 08	191	5.5	1.86	43.52	2.2[11]	11
NGC 4051	Sy 1.5	0.002336	12 03 10	+44 31 53	443	8.4	1.80	41.34	< 0.01[6]	4
NGC 4151	Sy 1.5	0.003320	12 10 33	+39 24 21	483	163.3	26.13	42.80	6.9[12]	12
NGC 4253	Sy 1.5	0.012929	12 18 27	+29 48 46	715	6.1	0.93	42.54	0.8[6]	4
4C +04.42	BL Lac	0.965	12 22 23	+04 13 16	690	4.5	0.80	46.58	?	7
NGC 4388	Sy 2	0.008419	12 25 47	+12 39 44	215	34.8	9.54	43.18	27[13]	13
NGC 4395	Sy 1.8	0.001064	12 25 49	+33 32 48	739	5.1	0.56	40.14	0.15[3]	4
3C 273	Blazar	0.15834	12 29 07	+02 03 09	655	34.2	5.50	45.58	0.5[4]	14
NGC 4507	Sy 2	0.011801	12 35 37	-39 54 33	152	14.9	6.46	43.30	29[6]	4
IGR J12391-1612	Sy 2	0.036	12 39 06	-16 10 47	83	1.4	3.46	44.02	1.9[11]	11
NGC 4593	Sy 1	0.009000	12 39 39	-05 20 39	723	20.1	3.31	42.78	0.02[6]	4
IGR J12415-5750	Sy 2	0.024	12 41 24	-57 50 24	440	1.1	0.33	42.64	?	15
3C 279	Blazar	0.53620	12 56 11	+05 47 22	497	3.6	0.82	45.97	≤ 0.13[3]	4
Coma Cluster	GClstr	0.023100	12 59 48	+27 58 48	516	7.2	1.09	43.11	< 0.01[4]	4
NGC 4945	Sy 2	0.001878	13 05 27	-49 28 06	276	33.8	9.85	41.88	400[6]	16
ESO 323-G077	Sy 2	0.015014	13 06 26	-40 24 53	761	6.9	1.20	42.78	55[17]	17
IGR J13091+1137	AGN	0.0251	13 09 06	+11 38 03	48	2.0	1.06	43.18	90[11]	15
NGC 5033	Sy 1.9	0.002919	13 13 28	+36 35 38	377	4.6	1.06	41.30	2.9[6]	4
Cen A	Sy 2	0.001830	13 25 28	-43 01 09	532	167.4	32.28	42.38	12.5[4]	16
MCG-06-30-015	Sy 1	0.007749	13 35 54	-34 17 43	567	4.9	0.73	41.99	7.7[6]	4
4U 1344-60	AGN	0.043	13 47 25	-60 38 36	603	16.6	2.83	44.09	2.19[6]	4
IC 4329A	Sy 1.2	0.016054	13 49 19	-30 18 36	440	41.7	8.19	43.68	0.42[6]	4
Circinus gal.	Sy 2	0.001448	14 13 10	-65 20 21	589	58.9	10.73	41.69	360[6]	16
NGC 5506	Sy 1.9	0.006181	14 13 15	-03 12 27	101	12.6	4.21	42.55	3.4[6]	4
NGC 5548	Sy 1.5	0.017175	14 18 00	+25 08 12	211[e]	2.4	0.71	42.67	0.51[6]	4
PG 1416-129	Sy 1	0.129280	14 19 04	-13 10 44	117	8.3	4.86	45.33	0.09[4]	4
ESO 511-G030	Sy 1	0.022389	14 19 22	-26 38 41	145	5.1	1.93	43.34	< 0.05[17]	17
IC 4518	Sy 2	0.015728	14 57 43	-43 07 54	338	2.3	0.49	42.44	?	4
IGR J16119-6036	Sy 1	0.016	16 11 54	-60 36 00	475	1.2	0.25	42.16	?	2
IGR J16482-3036	Sy 1	0.0313	16 48 17	-30 35 08	973	4.2	0.73	43.22	?	10
NGC 6221	Sy 1/2	0.004977	16 52 46	-59 13 07	523	5.6	1.32	41.86	1[18]	4
Oph Cluster	GClstr	0.028	17 12 26	-23 22 33	1763	30.8	4.10	43.90	?	25
NGC 6300	Sy 2	0.003699	17 17 00	-62 49 14	173	10.0	3.91	42.07	22[19]	16
GRS 1734-292	Sy 1	0.021400	17 37 24	-29 10 48	3332	45.9	4.03	43.62	3.7[4]	24
2E 1739.1-1210	Sy 1	0.037	17 41 54	-12 11 52	631	5.5	1.03	43.51	?	7
IGR J18027-1455	Sy 1	0.035000	18 02 47	-14 54 55	942	12.6	2.03	43.76	19.0[4]	20
PKS 1830-211	Blazar	2.507	18 33 40	-21 03 40	1069	12.7	2.07	48.02	≤ 0.7[3]	21
ESO 103-G35	Sy 2	0.013286	18 38 20	-65 25 39	36	4.2	2.97	43.07	15[3]	16
2E 1853.7+1534	Sy 1	0.084	18 56 00	+15 38 13	761	9.3	1.74	44.48	?	10

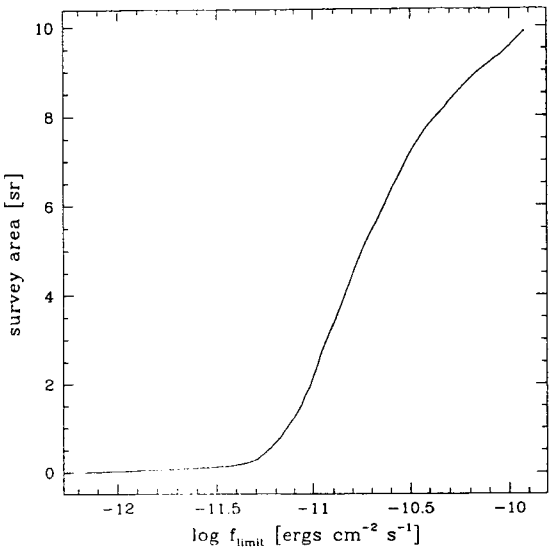

Fig. 3.— The total survey area with respect to the 5σ flux limit in the 20 - 40 keV band. For a flux limit of $f_X \geq 10^{-11}\,\mathrm{ergs\,cm^{-2}\,s^{-1}}$ the survey covers 76% of the sky, and for $f_X \geq 10^{-11}\,\mathrm{ergs\,cm^{-2}\,s^{-1}}$ 17%.

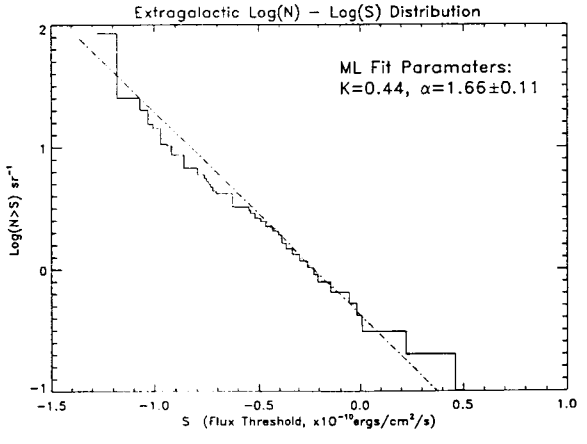

Fig. 4.— Number flux distribution per steradian of *INTEGRAL* AGN with a detection significance $> 5\sigma$. Blazars have been excluded. The maximum likelihood slope as described in Section 3.1 is 1.66 ± 0.11.

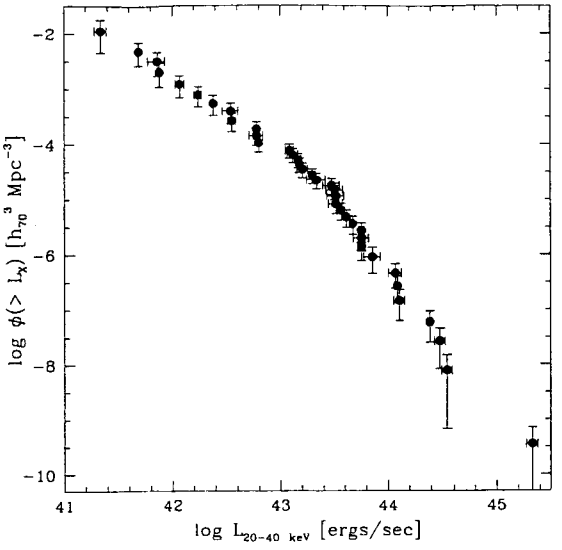

Fig. 5.— Cumulative luminosity function of *INTEGRAL* AGN with a detection significance $> 5\sigma$. Blazars have been excluded. The density ϕ describes the number of objects per Mpc^3 above a given luminosity L_X.

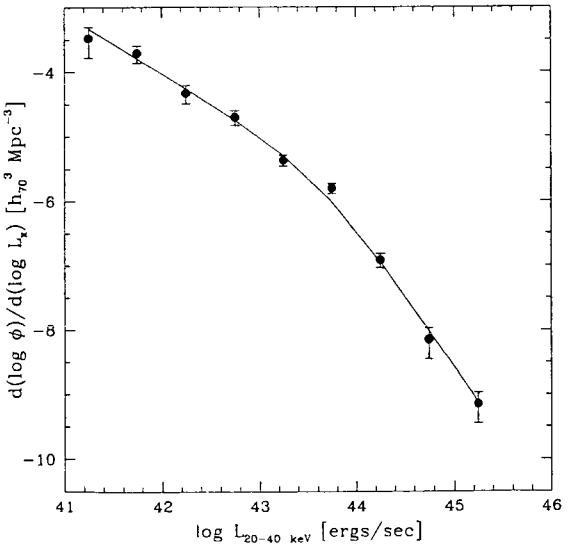

Fig. 6.— Differential luminosity function of AGN with $\Delta \log L_X = 0.5$ binning. The line shows a fit to a smoothly connected two power-law function with a turnover luminosity at $4.6 \times 10^{43}\,\mathrm{ergs\,s^{-1}}$.

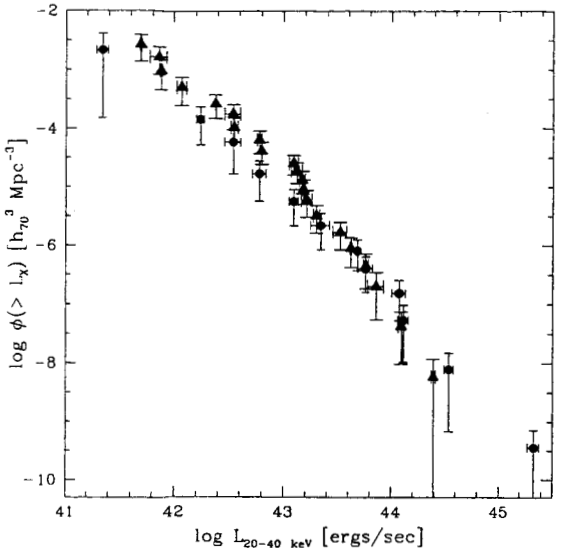

Fig. 7.— Cumulative AGN luminosity function for 21 absorbed ($N_H \geq 10^{22}\,\mathrm{cm}^{-2}$; triangles) and 13 unabsorbed sources (octagons).

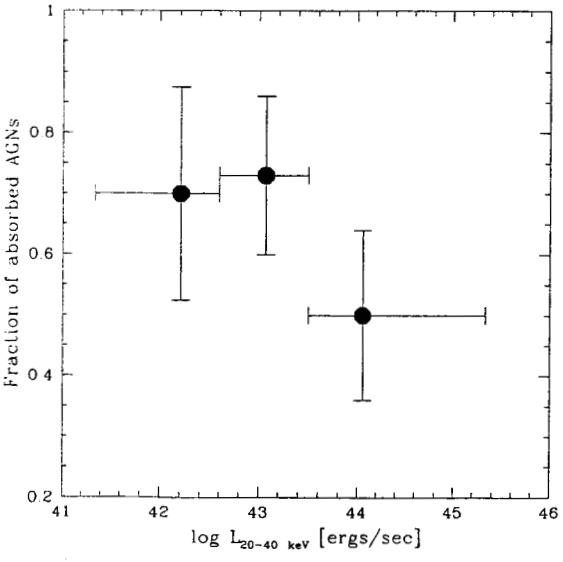

Fig. 8.— Fraction of absorbed AGNs ($N_H \geq 10^{22}\,\mathrm{cm}^{-2}$) versus luminosity. The position of the data point along the luminosity axis indicates the average luminosity in this bin, while the error bars in luminosity indicate the range of luminosities covered.

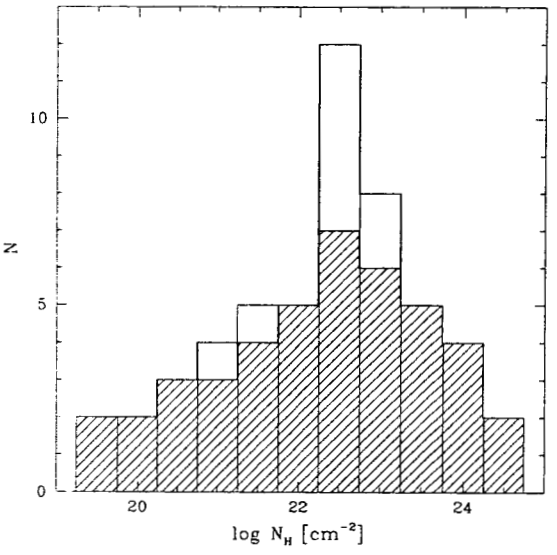

Fig. 9.— Distribution of intrinsic absorption for all *INTEGRAL* AGN (blazars excluded), as measured in the soft X-rays. The shaded area shows the reliable measurements, the other values are based on comparison of *ROSAT* All-Sky Survey and *INTEGRAL* data. Lower limits on absorption have been excluded.

TABLE 1—*Continued*

Name	Type	z	R.A. (J2000.0)	Decl. (J2000.0)	exp.[a] (ks)	ISGRI (σ)	f_X [b]	log $L_{20-40\,keV}$ (ergs s^{-1})	N_H [c,f]	Ref.[f]
1H 1934-063	Sy 1	0.010587	19 37 33	-06 13 05	684	2.7	0.48	42.08	?	4
NGC 6814	Sy 1.5	0.005214	19 42 41	-10 19 25	488	12.1	2.92	42.24	$< 0.05^3$	4
IGR J19473+4452	Sy 2	0.0539	19 47 19	+44 49 42	969	5.9	1.05	43.86	11^{11}	11
Cygnus A	Sy 2	0.056075	19 59 28	+40 44 02	1376	21.6	3.24	44.39	20^{22}	4
MCG +04-48-002	AGN	0.014206	20 28 35	+25 44 00	187	3.1	1.10	42.70	?	2
4C +74.26	AGN	0.0104	20 42 37	+75 08 02	72[e]	1.9	0.93	42.35	0.21^3	23
MRK 509	Sy 1	0.034397	20 44 10	-10 43 25	73	8.6	4.66	44.11	$< 0.01^3$	4
IGR J21247+5058	AGN	0.020	21 24 39	+50 58 26	213	11.9	4.15	43.57	?	20
3C 454.3	Blazar	0.859	22 53 58	+16 08 54	92[e]	2.8	3.1	46.56	?	26
MR 2251-178	Sy 1	0.063980	22 54 06	-17 34 55	489	7.0	1.20	44.07	$\leq 0.19^3$	4
MCG -02-58-022	Sy 1.5	0.046860	23 04 44	-08 41 09	489	3.9	1.20	43.79	$\leq 0.08^3$	4

[a]ISGRI exposure time

[b]flux $f_{(20-40\,keV)}$ in 10^{-11} erg cm^{-2} s^{-1}

[c]intrinsic absorption in 10^{22} cm^{-2}

[d]tentative redshift

[e]not covered by survey presented here

[f]REFERENCES.— (1) Donato, Sambruna, Gliozzi 2005; (2) Bassani et al. 2006; (3) Tartarus database; (4) Beckmann et al. 2006a; (5) Matt et al. 1997; (6) Lutz et al. 2004; (7) Bird et al. 2006; (8) Virani et al. 2005; (9) Pian et al. 2005; (10) Masetti et al. 2005; (11) Sazonov et al. 2005; (12) Beckmann et al. 2005; (13) Beckmann et al. 2004; (14) Courvoisier et al. 2003b; (15) Revnivtsev et al. 2005; (16) Soldi et al. 2005; (17) Sazonov & Revnivtsev 2004; (18) Levenson, Weaver, & Heckman 2001; (19) Matsumoto, Nava, Maddox et al. 2004; (20) Masetti et al. 2004; (21) De Rosa et al. 2005; (22) Young et al. 2002; (23) This work; (24) Sazonov et al. 2004; (25) Revnivtsev et al. 2004; (26) Pian et al. 2006